



Investigation of Response Amplitude Operators for Floating Offshore Wind Turbines

Preprint

G. K. V. Ramachandran, A. Robertson,
J. M. Jonkman, and M. D. Masciola

*To be presented at the 23rd International Ocean, Offshore and Polar Engineering Conference – ISOPE 2013
Anchorage, Alaska
June 30 – July 5, 2013*

**NREL is a national laboratory of the U.S. Department of Energy
Office of Energy Efficiency & Renewable Energy
Operated by the Alliance for Sustainable Energy, LLC.**

This report is available at no cost from the National Renewable Energy Laboratory (NREL) at www.nrel.gov/publications.

Conference Paper
NREL/CP-5000-58098
July 2013

Contract No. DE-AC36-08GO28308

NOTICE

The submitted manuscript has been offered by an employee of the Alliance for Sustainable Energy, LLC (Alliance), a contractor of the US Government under Contract No. DE-AC36-08GO28308. Accordingly, the US Government and Alliance retain a nonexclusive royalty-free license to publish or reproduce the published form of this contribution, or allow others to do so, for US Government purposes.

This report was prepared as an account of work sponsored by an agency of the United States government. Neither the United States government nor any agency thereof, nor any of their employees, makes any warranty, express or implied, or assumes any legal liability or responsibility for the accuracy, completeness, or usefulness of any information, apparatus, product, or process disclosed, or represents that its use would not infringe privately owned rights. Reference herein to any specific commercial product, process, or service by trade name, trademark, manufacturer, or otherwise does not necessarily constitute or imply its endorsement, recommendation, or favoring by the United States government or any agency thereof. The views and opinions of authors expressed herein do not necessarily state or reflect those of the United States government or any agency thereof.

This report is available at no cost from the National Renewable Energy Laboratory (NREL) at www.nrel.gov/publications.

Available electronically at <http://www.osti.gov/bridge>

Available for a processing fee to U.S. Department of Energy and its contractors, in paper, from:

U.S. Department of Energy
Office of Scientific and Technical Information
P.O. Box 62
Oak Ridge, TN 37831-0062
phone: 865.576.8401
fax: 865.576.5728
email: <mailto:reports@adonis.osti.gov>

Available for sale to the public, in paper, from:

U.S. Department of Commerce
National Technical Information Service
5285 Port Royal Road
Springfield, VA 22161
phone: 800.553.6847
fax: 703.605.6900
email: orders@ntis.fedworld.gov
online ordering: <http://www.ntis.gov/help/ordermethods.aspx>

Cover Photos: (left to right) photo by Pat Corkery, NREL 16416, photo from SunEdison, NREL 17423, photo by Pat Corkery, NREL 16560, photo by Dennis Schroeder, NREL 17613, photo by Dean Armstrong, NREL 17436, photo by Pat Corkery, NREL 17721.



Printed on paper containing at least 50% wastepaper, including 10% post consumer waste.

Investigation of Response Amplitude Operators for Floating Offshore Wind Turbines

G. K. V. Ramachandran, A. Robertson, J. M. Jonkman, and M. D. Masciola

National Wind Technology Center, National Renewable Energy Laboratory,
Boulder, CO, United States of America

ABSTRACT

This paper examines the consistency between response amplitude operators (RAOs) computed from WAMIT, a linear frequency-domain tool, to RAOs derived from time-domain computations based on white-noise wave excitation using FAST, a nonlinear aero-hydro-servo-elastic tool. The RAO comparison is first made for a rigid floating wind turbine without wind excitation. The investigation is further extended to examine how these RAOs change for a flexible and operational wind turbine. The RAOs are computed for below-rated, rated, and above-rated wind conditions. The method is applied to a floating wind system composed of the OC3-Hywind spar buoy and NREL 5-MW wind turbine. The responses are compared between FAST and WAMIT to verify the FAST model and to understand the influence of structural flexibility, aerodynamic damping, control actions, and waves on the system responses. The results show that based on the RAO computation procedure implemented, the WAMIT- and FAST-computed RAOs are similar (as expected) for a rigid turbine subjected to waves only. However, WAMIT is unable to model the excitation from a flexible turbine. Further, the presence of aerodynamic damping decreased the platform surge and pitch responses, as computed by both WAMIT and FAST when wind was included. Additionally, the influence of gyroscopic excitation increased the yaw response, which was captured by both WAMIT and FAST.

KEY WORDS: Floating offshore wind turbines; OC3-Hywind spar; response amplitude operator; RAO.

INTRODUCTION

Response amplitude operators (RAOs) are conventionally the frequency response functions, which are simply the ratio of the output to a given input. RAOs are used in the offshore oil and gas industry to assess the frequency-domain linear wave-body response of floating platforms during the design process. RAOs also have been applied in the design of floating platforms for wind turbines; but, in offshore floating wind turbines, in addition to the hydrodynamic loading, aerodynamics, structural dynamics (including blade and tower flexibility), and controller dynamics also are important effects. Due to the inherent nonlinearities of these dynamics, offshore floating wind turbines are designed and analyzed with nonlinear time-domain aero-

hydro-servo-elastic tools. It is important to understand how these additional dynamics affect the system responses. Due to sophistication of the nonlinear time-domain aero-hydro-servo-elastic tools, it also is essential that—before the models are applied in a design—the responses are verified as being meaningful. As such, it is important to compare the responses predicted from the complicated nonlinear time-domain tool to the responses predicted from a simpler model.

As floating wind turbines are receiving more attention, it is necessary to determine measures to describe the motion characteristics of each of the concepts when subjected to both wind and wave loading. A popular tool for computing RAOs of offshore platforms is WAMIT (Lee and Newman, 2006), a three-dimensional panel code used to compute the linear wave forcing and motion characteristics of an offshore structure in the frequency domain. However, the motion characteristics of a floating platform for a deep-water wind turbine are also influenced by the structural flexibility and the operational conditions of the wind turbine, including aerodynamics and controller-induced motion. It is not possible in WAMIT to capture the interaction of the flexible wind turbine degrees of freedom (DOFs) with the platform motion in the computation of RAOs or system nonlinearities. This is overcome by interfacing WAMIT with the nonlinear time-domain aero-hydro-servo-elastic code, FAST (Jonkman and Buhl, 2005), developed by the National Renewable Energy Laboratory (NREL). FAST can model the nonlinear dynamics of the flexible wind turbine subjected to hydrodynamic and aerodynamic excitation, and can compute the RAOs of the complete offshore wind system through white-noise wave excitation and the associated time-domain responses.

The purpose of this investigation is to verify the FAST/WAMIT model and to understand the influence of structural flexibility, aerodynamic damping, control actions, and waves on offshore floating wind system responses. To achieve this goal, RAOs generated from FAST/WAMIT are verified against WAMIT-only generated RAOs for a rigid offshore wind system. After the verification is completed, flexibility is added to the wind turbine in FAST and cases including wind excitation are used to understand the influence of these conditions on the RAOs.

The interaction of WAMIT and FAST for computing RAOs and performing the comparison process is shown in Figure 1. A detailed description of the RAO computation procedures using WAMIT and FAST is given in the next sections.

This report is available at no cost from the
National Renewable Energy Laboratory (NREL)
at www.nrel.gov/publications.

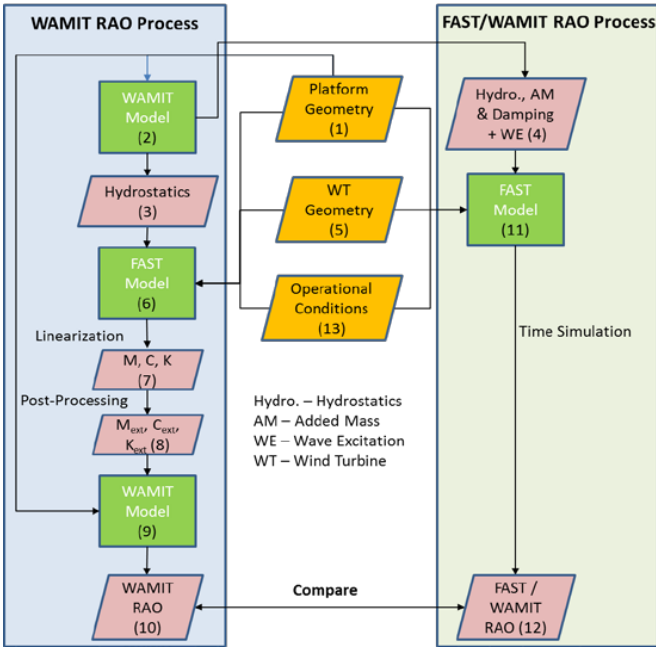


Figure 1. RAO computation flow chart

RESPONSE AMPLITUDE OPERATOR COMPUTATION PROCEDURE: WAMIT

WAMIT is a three-dimensional panel code used to compute the wave kinematics, wave forcing, and motion characteristics of an offshore structure in the frequency domain. WAMIT can provide the RAOs of a structure both in a freely floating condition and in a moored condition.

Here, WAMIT is used to produce RAOs for the complete offshore wind system, including the influences of the wind turbine and moorings. To obtain these RAOs, the geometry of the floating platform is modeled in WAMIT, and the influences of the turbine and moorings are supplied through external mass, stiffness, and damping matrices linked to the WAMIT model. The process of deriving these external matrices involves using FAST.

The WAMIT model-building process is as follows. First, the geometry of the floating platform is modeled in WAMIT and the hydrostatic quantities (without body gravity), added mass, damping, and wave-excitation forces of the system are computed assuming the platform as a freely-floating body. This information is used as input for a FAST model of the system, and is represented as blocks (1), (2), and (4) in the flow chart. For this computation, the center of gravity position is assumed to be at the intersection of the still water level (SWL) and the centerline of the platform/tower, so that WAMIT neglects the body gravity term when calculating the hydrostatic stiffness matrix in pitch and roll. This is done to avoid double-booking the body gravity term when the hydrostatic quantities are used by FAST, which intrinsically accounts for these contributions. In the WAMIT calculation of block (2), WAMIT does not see the wind turbine on top of the platform and hence the hydrodynamic and hydrostatic quantities are purely due to the interaction of the platform with the fluid.

Next, the complete floating system is modeled in FAST, which includes the hydrostatic quantities computed by WAMIT for a freely floating platform as input to the model. The FAST model is then used to derive the mass (\mathbf{M}), stiffness (\mathbf{K}), and damping (\mathbf{C}) matrices of the complete

system including the platform, wind turbine (including aerodynamics and rotor gyroscopic), and moorings through a linearization process, as shown in block (6). The FAST linearization is performed using the hydrostatic quantities from the previous step (block (3)), but with the hydrodynamics quantities (added mass and damping) zeroed out. Zeros are used for the hydrodynamic quantities to eliminate the hydrodynamic added mass and damping contribution and avoid double counting these contributions in the WAMIT RAO computation in block (9). The hydrostatic-restoring quantities, however, which don't include the body gravity term but do include the contributions of buoyancy and water-plane area, are needed by FAST in block (6) to ensure that the system is in static equilibrium before linearizing. For the FAST linearization computation in block (6) no waves are applied, mimicking a still-water condition. Appropriate wind conditions are applied based on the cases under investigation; hence, the corresponding aerodynamic loads influence the damping and stiffness matrices. Additionally, in the FAST linearization computation of block (6) the wind turbine is treated as a rigid body with only the six rigid-body degrees of freedom of the floating platform enabled. The resulting \mathbf{M} , \mathbf{C} , and \mathbf{K} matrices of size 6×6 derived by FAST in block (6) contain the effects of body mass/inertia, aerodynamics, gyroscopic, hydrostatics (contributions from both buoyancy and body weight), and mooring stiffness (in block (7)). These matrices are azimuth averaged for models with a rotating rotor.

In the third step, post-processing of the \mathbf{M} , \mathbf{C} , and \mathbf{K} matrices from block (7) is done in block (8) to eliminate any sort of double-booking. The post-processed matrices from block (8) are designated as the external matrices, \mathbf{M}_{ext} , \mathbf{C}_{ext} , and \mathbf{K}_{ext} , required by WAMIT to perform RAO computations in block (9). They include the influences of the wind turbine and moorings identified in the previous paragraph. The post-processing of the \mathbf{M} , \mathbf{C} , and \mathbf{K} matrices in block (8) is described next.

The external mass matrix, \mathbf{M}_{ext} , which contains the mass/inertia of the turbine, tower, and platform, is the same as that obtained from the FAST linearization output, \mathbf{M} , because the mass matrix does not include hydrodynamic added mass, as explained previously. If this was not the case, then the hydrodynamic mass matrix would need to be subtracted from the mass matrix, \mathbf{M} , to obtain the external mass matrix, \mathbf{M}_{ext} .

The external damping matrix, \mathbf{C}_{ext} , which includes the contributions from aerodynamic damping and gyroscopic effects, is also the same as that obtained from the FAST linearization output. For a non-spinning wind turbine with no aerodynamic loading and no platform viscous drag, the result should be a zero damping matrix, which can be used as a sanity check.

The stiffness matrix, \mathbf{K} —obtained from the FAST linearization output—contains the contributions from aerodynamics, hydrostatics, and gravitational and mooring line restoring, which is illustrated in the following equation:

$$\mathbf{K} = \mathbf{K}_{\text{aero}} + \mathbf{K}_{\text{hydrostat}} + \mathbf{K}_{\text{gravRest}} + \mathbf{K}_{\text{mooring}} \quad (1)$$

The external stiffness matrix, \mathbf{K}_{ext} , is obtained by excluding the hydrostatic stiffness contribution from the above equation. The hydrostatic restoring obtained from the first step in block (3) is used for this purpose. The computation of \mathbf{K}_{ext} is given in the following equation:

$$\mathbf{K}_{\text{ext}} = \mathbf{K} - \mathbf{K}_{\text{WAMIT}} \quad (2)$$

where, $\mathbf{K}_{\text{WAMIT}} = \mathbf{K}_{\text{hydrostat}}$ represents the hydrostatic stiffness matrix from block (3) obtained from the WAMIT computation of block (2).

The WAMIT output is non-dimensional; hence, $\mathbf{K}_{\text{hydrostat}}$ must be dimensionalized before applying the above equation.

In the final step, the RAOs are obtained from WAMIT in block (9) including the influences of the wind turbine and moorings. For this case, the external mass, damping, and stiffness matrices (\mathbf{M}_{ext} , \mathbf{C}_{ext} , and \mathbf{K}_{ext}) computed from FAST in block (6) and post-processed in block (8) are specified for setting up the equations of motion in WAMIT. Compared to the block (2) computation, the block (9) computation uses the \mathbf{M}_{ext} , \mathbf{C}_{ext} , and \mathbf{K}_{ext} matrices from block (8), representing the influence of the wind turbine and moorings. Solving the equations of motion in WAMIT gives rise to the linear motion responses of the structure. Each element in the external mass matrix is added to the corresponding added mass of the body (this addition is done by WAMIT internally) to obtain the complete mass matrix for the equations of motion. In the case of the damping and stiffness matrices, a similar process is performed, in which linear wave damping is added to the external damping matrix and the hydrostatic restoring contributions are added to the external stiffness matrix. The x, y, and z coordinates of the center of gravity (CG) location of the structure also must be specified in WAMIT, but are set to zero because the stiffness matrix from the third step (block (8)) contains the body gravity terms derived from FAST. The WAMIT computation in block (9) gives rise to the RAOs of block (10).

RESPONSE AMPLITUDE OPERATOR COMPUTATION PROCEDURE: FAST

The aero-hydro-servo-elastic code FAST computes the loads and responses of both onshore and offshore wind turbines. The procedure for computing the RAOs for a floating system using FAST is explained below.

FAST computes the system response nonlinearly in the time domain in block (11) of the flow chart, in contrast to the linearization in block (6) described in the previous section. The FAST computation is performed with both a rigid (resulting in only 6 DOFs) and a flexible wind turbine. In addition to the rigid-body motion of the floater, a flexible wind turbine includes degrees of freedom corresponding to blade and tower bending, rotor rotation, and drivetrain torsion.

The aerodynamic loads are calculated based on the controller settings and the wind conditions used. For the hydrodynamic loads, the WAMIT data from the first step of the previous section (represented in block (4)) are used in place of the zero-valued WAMIT data used as input to the FAST linearization. This data provides the frequency-dependent added mass and damping coefficients and the incident wave-excitation forces. The time-domain wave excitation for the RAO computation is described using a white-noise spectrum. Six sets of computations are carried out using white-noise excitations with six different seed numbers. Each of the computations is performed for a time duration of 8,000 s. The system responses from the six computations are averaged and the auto-spectral density of the input (wave elevation) and the cross-spectral density of the input/output (system responses) are computed in block (12). The ratio of the cross-spectral density of the surface elevation and the corresponding output to the auto-spectral density of the surface elevation gives rise to the frequency-response function (FRF), or the RAOs in block (12) (illustrated in the following equation):

$$RAO = H(\omega) = \frac{S_{xy}(\omega)}{S_{xx}(\omega)} \quad (3)$$

where, $H(\omega)$ is the FRF, $S_{xy}(\omega)$ and $S_{xx}(\omega)$ are the cross-spectral and auto-spectral densities of the input $x(t)$ and the output $y(t)$, in the frequency domain, respectively. The post-processing of the time series

results is performed by excluding the transients of the first 2,000 s from each computation. The process is repeated for different operational conditions (e.g., wind, wave) and degrees of freedom. These RAOs in block (12) are compared to those computed from WAMIT in block (10).

CASE STUDY: OC3-HYWIND SPAR-BUOY

The methods described above are implemented for a floating offshore wind turbine concept, namely the OC3-Hywind spar buoy (Jonkman, 2009), which is subjected to various wind and wave conditions. The NREL 5-MW reference wind turbine (Jonkman *et al.*, 2009) is mounted on the platform, which consists of a deep-drafted slender spar buoy with three mooring lines. The mooring lines are attached to the platform through a delta connection to achieve higher yaw mooring stiffness. FAST currently is not capable of modeling the delta connection; hence, an additional yaw stiffness of 9.834E7 Nm/rad is used to account for the simplification. Further, additional linear damping for surge and sway (1.0E5 N/(m/s)), heave (1.3E5 N/(m/s)), and yaw motions (1.3E7 Nm/(rad/s)) is applied to account for mooring damping neglected by FAST and to match with tank test data. For all the computations, the platform viscous drag is not considered (platform $C_d = 0$).

A schematic of the OC3-Hywind concept is shown in Figure 2. The specifications of the platform are presented in Table 1 (Jonkman, 2009) and the platform and tower natural frequencies are presented in Table 2 (Jonkman *et al.*, 2010) of the Appendix.



Figure 2. OC3-Hywind concept

As a first step, the RAOs computed using FAST and WAMIT are compared for a rigid turbine subjected to no wind. In FAST, white-noise waves with a significant wave height of 2 m are used, which is small enough that linear wave theory is valid. The results are shown in Figure 3. The RAOs show considerable excitation only in the surge, heave, and pitch modes, therefore only these RAOs are presented in the figure. The excitation at the other natural frequencies (sway, roll, and yaw) is considerably less because of the zero-degree wave heading and

the absence of wind forcing. The figure shows that the RAOs are in good agreement; however, a small frequency shift is present for the heave and pitch responses at their respective natural frequencies. The frequency shift could be due to a slight stiffening of the mooring lines in the FAST computation, wherein the nonlinearity of the catenary mooring is taken into account while the floater oscillates, which is not incorporated in the linearized WAMIT calculation. Further, the unity amplitude heave RAO corresponding to the zero-frequency limit—predicted by both of the tools—agrees very well, which is a sanity check for RAO estimation. (For an extremely long-period wave (long wavelength), the structure follows the wave in heave, which means that the output is the same as that of the input (excitation). This might not be the case for a tension leg platform (TLP); however, because TLPs are stiff structures.)

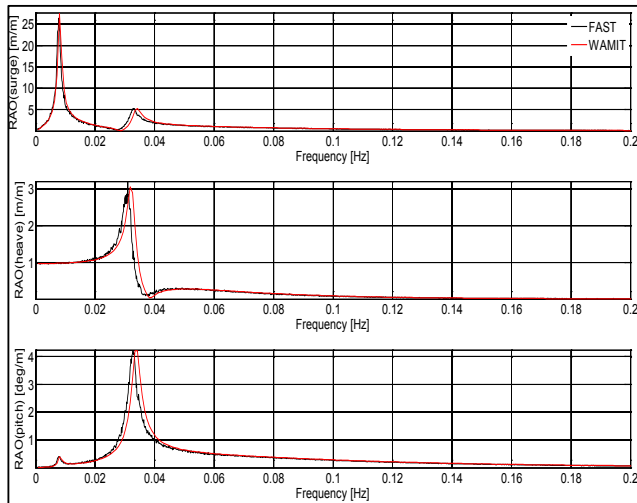


Figure 3. OC3-Hywind: RAO comparison (no-wind, rigid turbine)

This rigid case has verified the technique for deriving RAOs within FAST/WAMIT. The next step is to examine how these RAOs change due to both wind and flexibility of the turbine or tower. To examine the effect of these modifications, the following wind conditions are used:

- No wind (no aerodynamic loads are present)
- Below-rated steady wind speed at hub height, $V = 8 \text{ m/s}$
- Rated steady wind speed at hub height, $V = 11.4 \text{ m/s}$
- Above-rated steady wind speed at hub height, $V = 18 \text{ m/s}$

A variable speed/variable pitch controller developed for the OC3-Hywind system was used for the wind cases within FAST.

The RAOs are computed for these four wind cases within WAMIT alone by applying mass/stiffness/damping matrices that account for the influence of wind condition on the system. Eight different RAOs are computed in FAST, for each of the wind conditions and for both a rigid and flexible turbine/tower. The calculations in WAMIT are only for a rigid system. As in the previous example, a white-noise wave spectrum with a significant wave height of 2 m is used for the FAST computations. The results are shown in Figure 4 through Figure 9. In each, the main figure shows the low-frequency region of the RAO and the inset figure shows the relevant frequency of interest for each platform mode. The terms V0, V8, V11.4, and V18 represent the results corresponding to the steady wind speeds of $V = 0 \text{ m/s}$, $V = 8 \text{ m/s}$, $V = 11.4 \text{ m/s}$, and $V = 18 \text{ m/s}$, respectively. Further, the “flex” and

“rigid” keywords for FAST represent that the wind turbine is considered “flexible” and “rigid”, accordingly.

Figure 4 shows the comparison of surge RAOs. From the figure, as expected, all the RAOs compare well at around the surge natural frequency (0.008 Hz). Additionally, as compared to the other cases, the surge natural frequency for the flexible turbine RAO corresponding to the rated wind speed has slightly higher amplitude and a lower frequency. It can also be noted that the no-wind case RAO (both rigid and flexible turbines) shows only the surge-pitch coupling through the peak at the pitch natural frequency (0.034 Hz), whereas the RAOs at the operational conditions show both surge-heave and surge-pitch couplings through the excitation peaks at 0.032 Hz and 0.034 Hz, respectively. Further, the peak corresponding to the surge-pitch coupling of the no-wind case is much higher in amplitude than that of the operational condition RAOs, due to the absence of aerodynamic damping for the no-wind case RAOs. A smaller peak is observed (but is not shown in the figure) at about the first blade flap-wise natural frequency (0.63 Hz) for the flexible-turbine case in FAST (but not in WAMIT, which cannot model turbine flexibility).

Similar to Figure 4, the sway RAOs are compared in Figure 5, which show small excitations at the sway natural frequency (0.008 Hz) and at the roll natural frequency (0.034 Hz), demonstrating the sway-roll coupling. For a zero-degree steady wind and wave heading, the sway response is expected to be minimal (and can be observed in the figure), because the sway motion is excited only by rotor torque and transverse aerodynamic loads brought about by rotor gyroscopic-induced yaw motion. The magnitudes of the no-wind RAOs are very small as compared to the operational cases, because of the absence of rotor loads. Further, the operational case responses (between the wind speed conditions of 8, 11.4, and 18 m/s) are comparable in magnitude, but increase slightly with increasing wind speed, which is the result of higher aerodynamic torque. Additionally, the influence of aerodynamic damping is not present in this degree of freedom. Smaller peaks at the first tower side-side frequency (0.46 Hz) and at the first coupled blade flap-wise bending frequency (0.65 Hz) are visible for the FAST RAOs in the case of a flexible turbine.

The heave RAO comparison is shown in Figure 6. The heave RAOs compare well at the heave natural frequency (0.032 Hz). This is because the heave response at its natural frequency is unaffected by the aerodynamic damping.

Figure 7 presents the roll RAO comparison. It shows a behavior similar to that of the sway response. The roll-sway coupling is also visible.

The pitch RAOs are compared in Figure 8. Similar to the surge, the no-wind case RAOs compare well at the pitch natural frequency (0.034 Hz). The operational case RAOs also compare well at the pitch natural frequency, but with a smaller magnitude as compared to that of the no-wind case RAOs. This shows the influence of the aerodynamic damping. All the RAOs show the surge-pitch coupling through the peak at the surge natural frequency. Further, all the operational case RAOs show the heave-pitch coupling through a peak at the heave natural frequency. This is not present for the no-wind case RAO, as seen in the surge response case. The flexible turbine RAOs show a peak at about 0.47 Hz, corresponding to the first fore-aft tower frequency. Further, the peak at the tower frequency is slightly shifted in cases that include wind compared to that of the no-wind condition, which may be attributed to the additional aerodynamic stiffness or stiffening of the mooring system to the aerodynamic-thrust-induced mean surge offset.

Figure 9 shows the yaw RAO comparison. None of the WAMIT-computed RAOs has an excitation at the yaw natural frequency

(0.121 Hz), which is due to the fact that hydrodynamic yaw forcing is zero for a cylindrical structure and the main cause for this excitation should come from the rotor aerodynamics, especially the rotor flexibility. This is clearly visible for the FAST-computed RAOs as excitation at the yaw natural frequency. All the RAOs show excitations at the surge / sway and roll / pitch natural frequencies demonstrating the yaw coupling with these DOFs. Further, all the FAST-computed RAOs during operational conditions show an excitation close to 0.6 Hz, corresponding to the 3p excitation (a rated rotor speed of 12.1 rpm gives rise to a 1p frequency at around 0.2 Hz) from the rotor. This effect is more predominant for the rated and above rated wind speed conditions. The flexible turbine RAOs show a peak at around 0.46 Hz, corresponding to the first tower side-side frequency and demonstrating the coupling between the platform yaw motion and the tower bending flexibility.

CONCLUSIONS

Two procedures are explained for computing the RAOs of floating wind turbines using WAMIT and FAST. A comparison of RAOs computed for a rigid turbine by both WAMIT and FAST (using white-noise wave excitation) shows that WAMIT can be used as a verification tool for the modeling of floating wind turbines in FAST. The RAOs for a flexible turbine, however, cannot be estimated using WAMIT.

Further, the comparison of RAOs for different wind conditions shows the influence of aerodynamic damping and gyroscopic effect. Although the presence of aerodynamic damping decreased the surge and pitch responses, the influence of gyroscopic loading increased the yaw response. The rigid and flexible turbine responses also are comparable, but the high-frequency excitations observed for the flexible turbine are larger than that of the rigid turbine.

The results also show different platform degrees of freedom coupling effects, such as surge-heave, surge-pitch, sway-roll, rotor gyroscopies–platform yaw, and platform yaw–tower bending flexibility. Most of the platform–turbine coupling is captured only using FAST, because the turbine flexibility could not be included in the WAMIT computation.

The analysis presently is being extended for tension-leg and semi-submersible platforms. It is expected that the impact of the turbine (especially tower) flexibility will be much more important for tension-leg platforms due to the strong coupling between platform-pitch and tower-bending (Matha, 2009).

ACKNOWLEDGEMENTS

This work was supported by the U.S. Department of Energy, under Contract No. DE-AC36-08GO28308 with the National Renewable Energy Laboratory.

REFERENCES

- Jonkman, JM (2009). *Definition of the Floating System for Phase IV of OC3*, TP-500-47535. Golden, CO: National Renewable Energy Laboratory.
- Jonkman, JM, and Buhl, ML (August 2005). *FAST User's Guide*, EL-500-38230. Golden, CO: National Renewable Energy Laboratory.
- Jonkman, J, Butterfield, S, Musial, W, and Scott, G (February 2009). *Definition of a 5-MW Reference Wind Turbine for Offshore System Development*, TP-500-38060. Golden, CO: National Renewable Energy Laboratory.
- Jonkman, J, Larsen, T, Hansen, A, Nygaard, T, Maus, K, Karimirad, M, Gao, Z, Moan, T, Fylling, I, Nichols, J, Kohlmeier, M, Pascual Vergara, J, Merino, D, Shi, W, and Park, H (2010). "Offshore Code Comparison Collaboration Within IEA Wind Task 23: Phase IV Results Regarding Floating Wind Turbine Modeling," *Proceedings of the European Wind Energy Conference—EWEC2010*, Warsaw, Poland.
- Lee, CH, and Newman, JN (2006). *WAMIT User Manual, Versions 6.4, 6.4PC, 6.3S, 6.3S-PC*, WAMIT, Inc., 343 pp.
- Matha, D (2009). *Model Development and Loads Analysis of an Offshore Wind Turbine on a Tension Leg Platform, with a Comparison to Other Floating Turbine Concepts*, MS Thesis, Endowed Chair of Wind Energy, Universität Stuttgart, Germany. Available at <http://www.nrel.gov/docs/fy10osti/45891.pdf> (accessed March 15, 2013).

APPENDIX

Table 1. OC3-Hywind Platform Specifications¹

Parameter	Value
Water depth (m)	320
Diameter (m)	6.5 to 9.4 (tapered)
Draft (m)	120
Water displacement (m ³)	8029
Mass, including ballast (kg)	7,466,000
Center of gravity location of the platform below still water level (m)	89.92
Roll inertia about center of gravity (kg-m ²)	4,229,000,000
Pitch inertia about center of gravity (kg-m ²)	4,229,000,000
Yaw inertia about center of gravity (kg-m ²)	164,200,000
Number of mooring lines	3
Depth to fairleads, anchors (m)	70
Radius to fairleads, anchors (m)	5.2
Unstretched line length (m)	902.2
Line diameter (m)	0.09
Line mass density (kg/m)	77.71
Line extensional stiffness (N)	384,200,000
1. The mass, center of gravity, and inertia values are for the platform alone (not including the tower and turbine).	

Table 2. OC3-Hywind Platform and Tower Natural Frequencies

Mode	Natural Frequency (Hz)
Surge	0.008
Sway	0.008
Heave	0.032
Roll	0.034
Pitch	0.034
Yaw	0.121
Tower first side-side	0.457
Tower first fore-aft	0.473

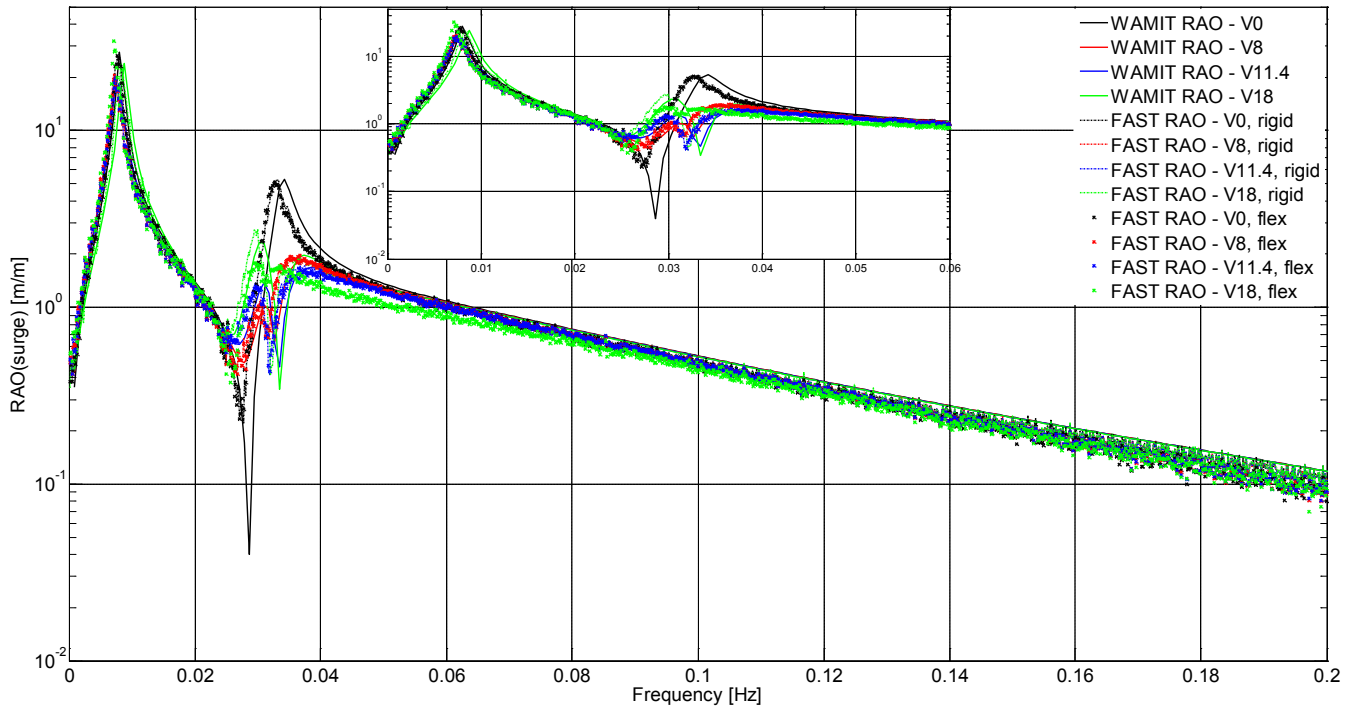


Figure 4. OC3-Hywind: Surge RAO comparison (main figure shows the low-frequency region of the RAO; inset figure shows relevant frequency)

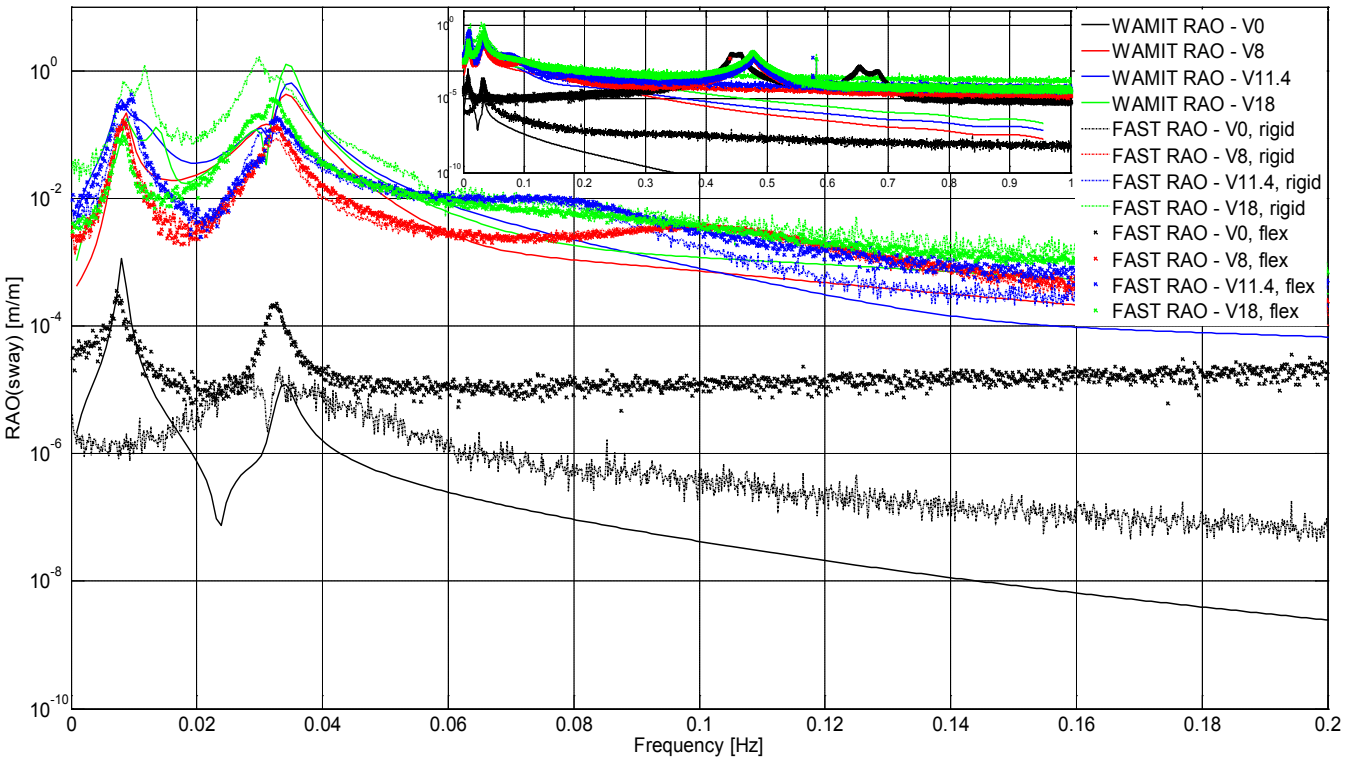


Figure 5. OC3-Hywind: Sway RAO comparison (main figure shows the low-frequency region of the RAO; inset figure shows relevant frequency)

This report is available at no cost from the
National Renewable Energy Laboratory (NREL)
at www.nrel.gov/publications.

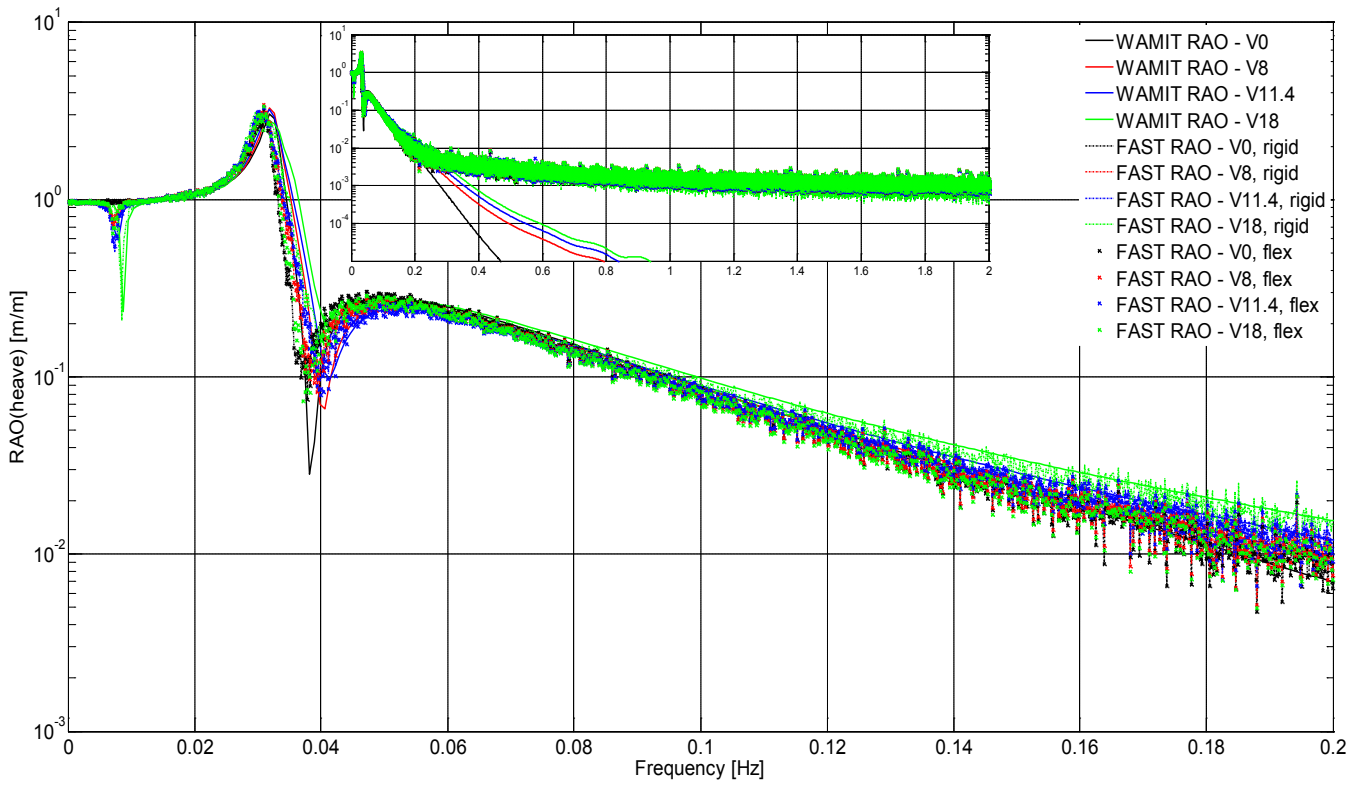


Figure 6. OC3-Hywind: Heave RAO comparison (main figure shows the low-frequency region of the RAO; inset figure shows relevant frequency)

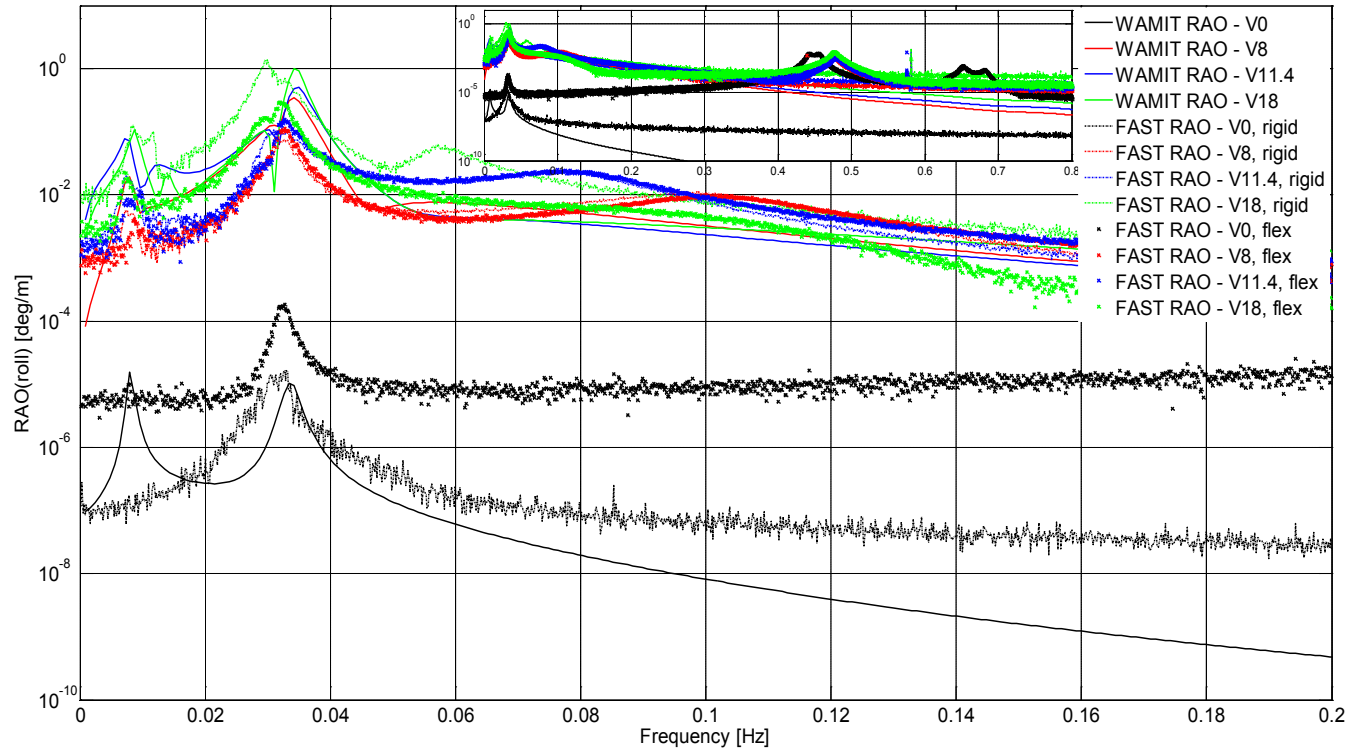


Figure 7. OC3-Hywind: Roll RAO comparison (main figure shows the low-frequency region of the RAO; inset figure shows relevant frequency)

This report is available at no cost from the
National Renewable Energy Laboratory (NREL)
at www.nrel.gov/publications.

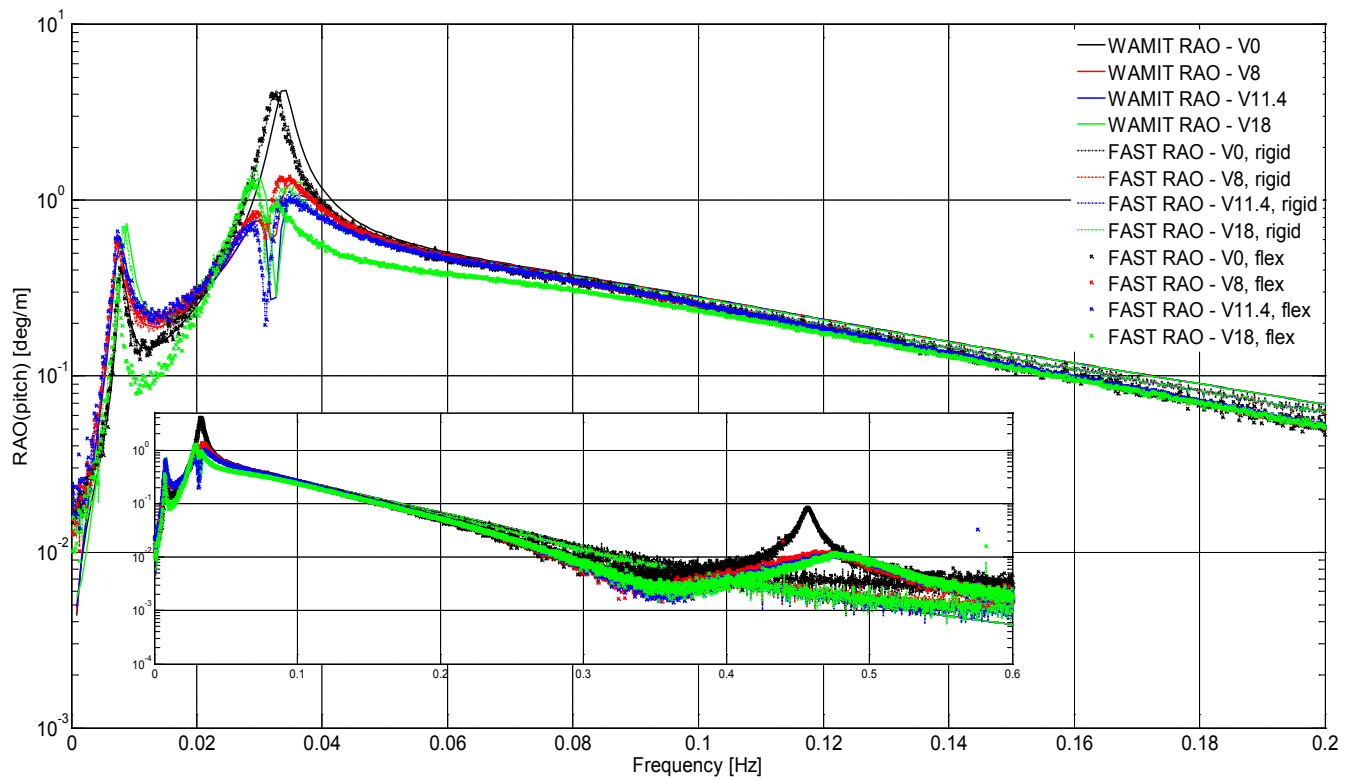


Figure 8. OC3-Hywind: Pitch RAO comparison (main figure shows the low-frequency region of the RAO; inset figure shows relevant frequency)

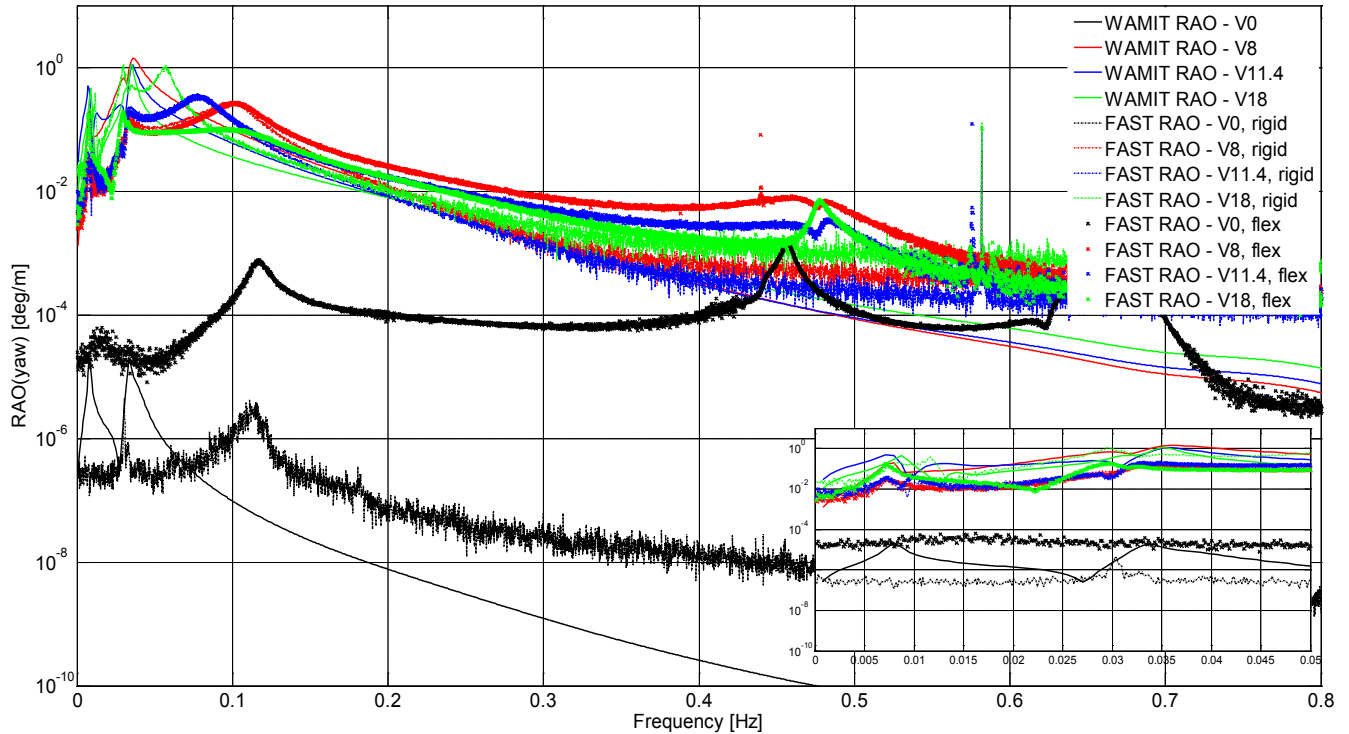


Figure 9. OC3-Hywind: Yaw RAO comparison (main figure shows the low-frequency region of the RAO; inset figure shows relevant frequency)

This report is available at no cost from the
National Renewable Energy Laboratory (NREL)
at www.nrel.gov/publications.